The effects of turbulence intensity on the downstream performance of horizontal axis tidal stream turbines

5 authors, including:

Ian Masters
Swansea University
104 PUBLICATIONS   **1,124** CITATIONS

SEE PROFILE

Alison J. Williams
Swansea University
48 PUBLICATIONS   **676** CITATIONS

SEE PROFILE

Matt Edmunds
Swansea University
18 PUBLICATIONS   **175** CITATIONS

SEE PROFILE

Parakram Pyakurel
Florida Atlantic University
16 PUBLICATIONS   **70** CITATIONS

SEE PROFILE

Some of the authors of this publication are also working on these related projects:

Project   Sêr Cymru National Research Network for Low Carbon, Energy and the Environment View project

Project   EWTEC conference View project

THE EFFECTS OF TURBULENCE INTENSITY ON THE DOWNSTREAM PERFORMANCE OF HORIZONTAL AXIS TIDAL STREAM TURBINES.

I. Masters[*], A. J. Williams[*], M. Edmunds[*], P. Pyakurel[†] J. H. VanZwieten[†]

[*]Marine Energy Research Group, Energy and Environment Research Group,
Zienkiewicz Centre for Computational Engineering,
College of Engineering, Swansea University,
Swansea, Wales, UK.
e-mail: I.Masters@swansea.ac.uk, web page: http://www.swansea.ac.uk

[†] Florida Atlantic University
Florida, USA.
e-mail: jvanzwi@fau.edu, web page: http://www.fau.edu

Key words: Computational methods, marine Eengineering, tidal stream turbine, marine currents, turbulence, wake, computational fluid dynamics

Abstract. This study focuses on a comparison of model results from a blade element momentum computational fluid dynamics (BEM-CFD) steady state RANS model, and a BEMT model that accounts for the wake generated from upstream turbines using analytic expressions. Rotor forces are calculated using 3D hydrofoil profile data. Both techniques are validated against existing experimental data, and then used to assess the power extraction of downstream turbines. Turbulent inflow conditions of 3% and 7% are applied, and the results of power extraction assessed. Particular attention is paid to the velocity field, with respect to the downstream wake, to assess how the turbulence characteristics effect the recovery rate and downstream power potential. Both models highlight the different recovery rates of the two turbulent conditions.

1   INTRODUCTION

This study focuses on two approaches for the prediction of tidal stream energy extraction. One approach is the BEM-CFD steady state RANS model [1] which computes the rotor forces acting on the fluid from lift, drag, and geometric data supplied to the model as inputs. The velocity and turbulence fields are also predicted. The second approach utilises a BEMT model [2] that accounts for the wake generated from upstream turbines using analytic expressions for mean flow and turbulent wake properties. Rotor forces are calculated using 3D lift and drag, and a dynamic wake model is implemented.

To study the effects of turbulence on performance, the models are validated against existing experimental data [3], and then used to assess the power extraction of downstream turbines. A

range of turbulent inflow conditions are applied, and the results of power extraction assessed. Particular attention is paid to the velocity field, with respect to the downstream wake, to assess how the turbulence characteristics effect the recovery rate and downstream power potential.

The remainder of this paper describes the models, case setups, results, and conclusions. Section 2 describes the BEMT analytical wake field expression, this is then followed in Sections 3.1 and 3.2 with a discussion of the BEM-CFD model. In Section 4 the modelled cases are described. The results are then discussed in Section 5, and are followed by conclusions in Section 6.

2 Analytical Wake Field Expression

Empirical expressions have been developed to approximate the wake field behind horizontal axis tidal turbines in the far-wake region. These expressions represent the reduced flow speed using expressions originally developed for wind turbines [4], with coefficients optimised using experimentally measured flow speeds behind horizontal axis tidal turbine [5]. These expressions define velocity deficit in the far-wake as a function of thrust coefficient and ambient turbulence intensity [5]. Expressions for downstream turbulence intensities have also been developed and tuned by [5]. These expressions were not directly derived from wind wake models, but were created such that they are a function of the same two operating parameters; thrust coefficient and ambient turbulence intensity. For lower ambient turbulence intensities, such as the 3% and 7% ambient values used in this study, it was shown by [5] that expressions based on the Larsen model [6] are well suited for calculating centreline velocity deficit and those based on the Ainslie model [7] effectively describe the dependence on radial location. This model is referred to as the Larsen/Ainslie model by [4].

The Larsen/Ainslie expression described by [4] defines velocity deficit in the far wake region according to:

$$\frac{U_w}{U_o} = 1 - U_c^* e\left(-3.56\left(\frac{r}{2r_o b}\right)^2\right) \tag{1}$$

where r is the radial distance from turbine centreline, r_o is the radius of rotor, U_o is the free stream velocity,

$$b = \left[\frac{3.56C_T}{8U_c^*(1 - 0.5U_C^*)}\right]^{\frac{1}{2}} \tag{2}$$

and

$$U_c^* = \frac{1}{9}\left(C_T A_d x^{-2}\right)^{\frac{1}{3}}\left(\left(\frac{35}{2\pi}\right)^{\frac{3}{10}}\left(3c_1^2\right)^{-\frac{1}{5}}\right)^2 \tag{3}$$

In these equations C_T is the thrust coefficient, A_d is the rotor area, x is the distance in the downstream direction (x axis), and c_1 is non-dimensional mixing length (empirical coefficient) defined by [5] as:

$$c_1 = 0.0406e^{0.1361TI} \tag{4}$$

where TI is the ambient turbulence intensity. It is suggested by [5] that this algorithm only be utilised within the wake radius suggested by Jensen [8] as:
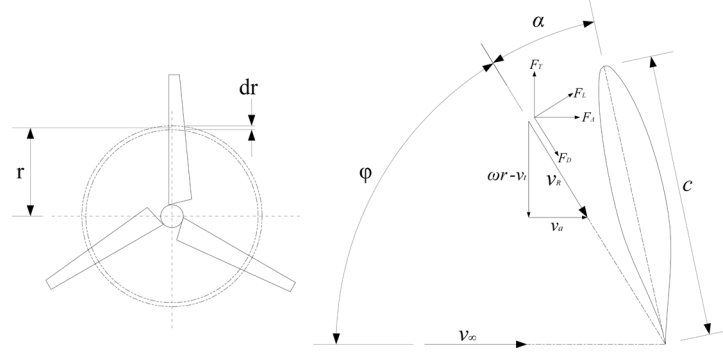
$$r_x = r_o + \alpha x \tag{5}$$

Figure 1: Blade element method rotor discretisation scheme.

where $\alpha = 0.00003TI^4 - 0.0009TI^3 + 0.0097TI^2 - 0.0396TI + 0.0763$. After this wake radius it is suggested that ambient flow speeds should be utilised.

The empirical expression for calculating the turbulence intensity in the far-wake region suggested by Pyakurel [5] defines turbulence intensity according to:

$$TI_w = TI\left(\left(\frac{TI_c - TI}{TI}\right)e^{-3\left(\frac{r}{D}\right)^2} + 1\right)$$ (6)

where TI_c is the centreline turbulence intensity calculated according to:

$$TI_c = \sqrt{\Delta TI^2 + TI^2}$$ (7)

In this equation the increased turbulence intensity at the centreline is calculated from:

$$\Delta TI^2 = \frac{1.5}{TI^{0.15}}C_t{}^{0.4}\left(\frac{x}{D}\right)^k$$ (8)

where $k = -2TI^{0.1}$.

3   BEM-CFD

This section introduces the hybrid analytical, BEM, and CFD computational model. First is a short discussion of the CFD process, governing equations and turbulence models (Section 3.1). The following section outlines the BEM-CFD approach (Section 3.2), as described by [1], and validated against [3].

3.1   CFD and the Governing Equations

CFD simulations are conducted using OpenFOAM [9]. Linking the CFD flow domain to the BEM model is achieved by additional source terms included within the conservation of momentum equations of the solver. The solver uses steady state Reynolds averaged incompressible Navier-Stokes equations with a range of turbulence model options including K-Epsilon, K-Epsilon RNG, and K-Omega.
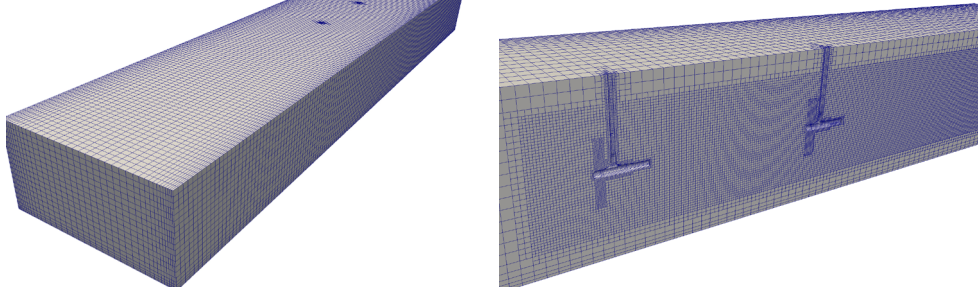
Figure 2: This figure shows the mesh generated using a combination of 'blockMesh' and 'snappy-HexMesh' utilities. The left image shows the outer/base distribution of cells, while the right image shows the refinements made around the wake and rotor regions.

The CFD model requires the solution of the Navier Stokes equations representing the conservation of mass and momentum. These equations are expressed as follows:

$$\nabla \cdot (\rho \vec{v}) = 0 \tag{9}$$

$$\nabla \cdot (\rho \vec{v} v_i) = -\frac{\partial p}{\partial x_i} + \nabla \cdot ([\mu_l + \mu_t]\nabla[\rho v_i]) + S_i \tag{10}$$

where ρ is the density, $\vec{v}$ is the velocity vector, v_i is the ith component of the velocity vector, μ_l and μ_t are the laminar and turbulent dynamic viscosities respectively, and S_i includes an additional source representing the moving rotor.

A widely used method for simulating the effect of turbulence on the mean flow, at the sub grid level, is the k-ϵ turbulence model [10]. Although this model is relatively simple, stable, and requires modest computational cost, it is limited by the single length scale used to calculate the viscous properties of the turbulent fluctuations. Diffusion, as a result of the turbulent fluctuations, does not occur at just one length scale. The k-ϵ RNG model [11] tries to address this issue by utilising statistical analysis to describe the set of turbulent length scales. Although these models regard turbulence as being isotropic in nature, in rotational flow, such as found in turbine wakes, the turbulent eddies are likely anisotropic. In this work the focus on performance of turbine rotors, rather than flow structures of the highly turbulent near wake region immediately downstream of the device, justifies the use of the k-ϵ RNG model.

In this model two equations are solved; k represents the energy contained within the turbulent fluctuations, and ϵ represents the dissipation rate of this energy. The equations for the transport of these variables are similar in form to the momentum equations:

$$\nabla \cdot (\rho \vec{v} k) = \nabla \cdot \left(\left[\mu_l + \frac{\mu_t}{\sigma_k} \right] \nabla k \right) + \mu_t G - \rho \epsilon \tag{11}$$

$$\nabla \cdot (\rho \vec{v} \epsilon) = \nabla \cdot \left(\left[\mu_l + \frac{\mu_t}{\sigma_\epsilon} \right] \nabla \epsilon \right) + C_{1\epsilon} \mu_t G \frac{\epsilon}{k} - C_{2\epsilon} \left(\frac{C_\mu \eta^3 [1 - \eta/\eta_0]}{1 + \beta \eta^3} \right) \tag{12}$$

where:

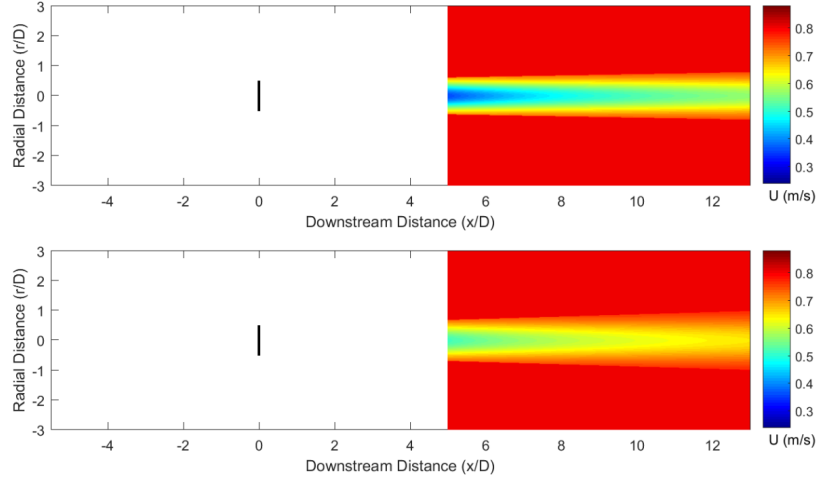$$\eta = \sqrt{G} \frac{k}{\epsilon} \tag{13}$$

Figure 3: BEMT analytical mean wake velocity in the far wake region behind horizontal axis tidal turbines for turbulence intensities of 3% (top) and 7% (bottom).

These equations are used to calculate a turbulent viscosity:

$$\mu_t = \frac{\rho C_\mu k^2}{\epsilon} \tag{14}$$

In Equations 11, 12, and 14; σ_k, σ_ϵ, $C_{1\epsilon}$, $C_{2\epsilon}$, C_μ, β, and η_0 are taken to be constants, and G represents the turbulent generation rate. The viscosity components of the k and ϵ equation diffusion terms, are effectively the sum of the laminar and turbulent viscosities.

3.2 The BEM-CFD Method

Fluid flowing over the surface of a body has a force exerted on it. Of interest, when describing hydrofoils, are the lift and drag components of this force, see Figure 1. Lift is defined as a force perpendicular to the free stream flow direction. Drag is defined as being parallel to, and opposing, the free stream flow direction. These hydrodynamic forces can be described by the following equations:

$$F_L = 0.5\rho\vec{v}^2 A C_L \tag{15}$$

$$F_D = 0.5\rho\vec{v}^2 A C_D \tag{16}$$

where F_L is lift force, and F_D is drag force, ρ is fluid density, $\vec{v}$ is velocity, A is area, C_L is the coefficient of lift, and C_D is the coefficient of drag. The coefficients of lift and drag are dependant on the angle of attack, α, the geometric properties of the hydrofoil, and the Reynolds Number. Data for a wide range of profiles is available from a number of sources including [12]. The chord and twist geometric properties, in combination with the profile C_L and C_D characteristics, are a function of the overall rotor design/performance requirements.

The influence of a tidal turbine with multiple hydrofoils (or blades) is averaged over a rotational interval, i.e. the rotor applies the same force to all locations at the same radial distance
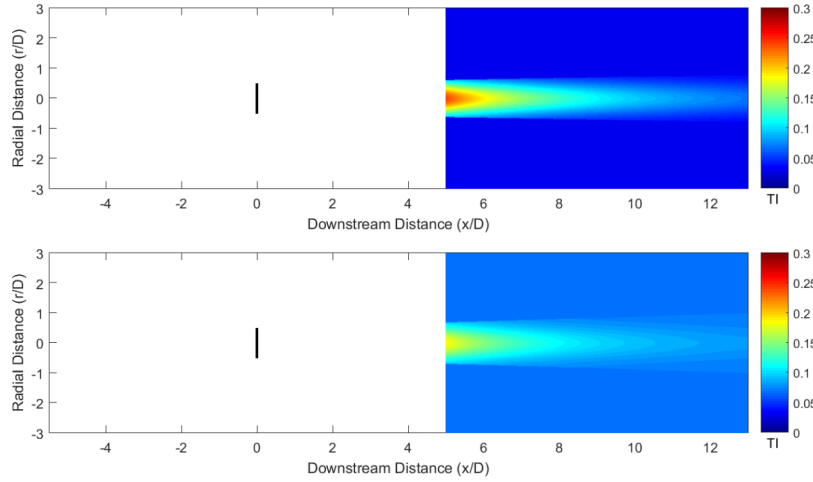
Figure 4: BEMT analytical turbulence intensity in the far wake region behind an horizontal axis tidal turbine for turbulence intensities of 3% (top) and 7% (bottom).

from the rotor centre on a given axial plane. The magnitude of these forces are a function of the hydrofoil geometry, its hydrodynamic properties, the quantity of hydrofoils, and their speed relative to the flow.

The BEM-CFD model is formulated such that the relevant characteristics of the hydrofoil are introduced through additional source terms appended to the momentum equation, see Section 3.1. Figure 1 shows how a turbine with three hydrofoils is discretised for use with the blade element method. The hydrofoil properties are determined at radius r_i, and then averaged over 2π radians. This process is repeated for each hydrofoil element over the interval $[r_0, r_{max}]$. For a detailed examination and validation of this approach, including tip loss correction, the reader is referred to [1].

4 Model Setup

The model described in Section 3.2 is implemented in OpenFOAM [9]. In this section is described the model setup including; mesh configuration, boundary conditions, and initial conditions, with respect to the OpenFoam Toolbox.

4.1 Case Studies

Investigations by [13, 14] evaluate horizontal axis tidal turbine performance, while studies by [15, 16, 17, 18, 19, 20] validate analytical or numerical models with experimental results. The work by [3] and [21] is of particular interest for the validation of this work. In this research the experimental work of [3] and [21] for a single and dual tidal turbines are compared with BEMT and BEM-CFD. The case studies are set such that the geometry of the turbines, and the domain extents, match that of the experimental studies.

In support of this study two turbulence cases are examined. Turbulence intensity (TI) is set at the inlets and allowed to dissipate to meet the required quantity at the centre rotor. The target TI for the two cases is 3% and 7% at the rotor. This required a TI setting of 5% and
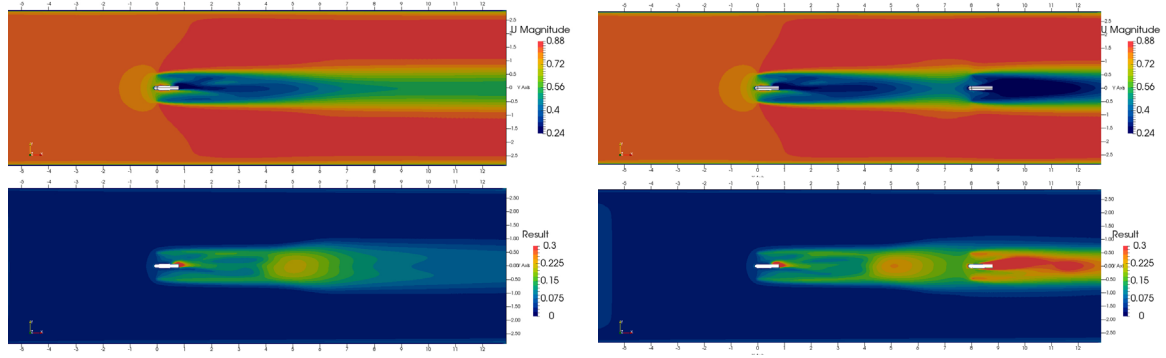
Figure 5: Top images are of velocity magnitude , while the bottom images are of turbulence intensity at 3%. The left images are of the single rotor case, and the right images are of the dual rotor case. All plots are taken in the horizontal plane at hub height, and the axis units are in diameters.

8% respectively to be set at the inlet. A matrix of full TSR sweeps [1...7] is run for each of the turbulence and single/dual rotor cases. The front rotor for all 8 diameter spaced dual rotor cases is held at TSR4. A single run of TSR3.67 front and rear rotor is also run for each turbulence case at 4 diameter spacing.

4.2 Mesh Configuration

Using the blockMesh utility, the mesh domain is configured as a hexahedron with bounding points [-9, -2, -1] to [9, 2, 1] which captures the domain extents of 18m x 4m x 2m in x, y, and z [3]. The domain is then subdivided in by [150, 40, 20]. Simple grading is used to refine the mesh to 0.2m at the left, right, and bottom boundaries, see Figure 2.

Refinement of the mesh around the turbines and wake region is achieved using the snappyHexMesh utility. The wake region is defined as a cylinder 0.7m radius, extending from 0.7m in front of the rotor to the end of the domain. The refinement level in this region is specified as level 2. The rotor assemblies are set with a refinement level of 3, see Figure 2.

Three arrangements of mesh are generated for this study. One has a single turbine at [0,0,0], one has 2 turbines where the second is set at 4 diameters (2.8m) downstream, and one has 2 turbines where the second is set at 8 diameters (5.6m) downstream. The boundary layer height at the turbine geometry is set to 0.2m, providing a cell centre height (0.1m) which achieves a $y+$ of ≈ 150.

4.3 Initial and Boundary Conditions

The initial conditions (and inlet condition) for velocity is set to 0.8m/s. Fixed value of 0.0m/s are set at the boundaries except the top and outlet, which are set to slip and zero gradient respectively. Kinetic energy and dissipation rate are set similarly and use wall functions to compute the boundary layer. The kinetic energy initial condition and inlet is set to $0.0024 m^2.s^{-2}$ (for the 3% TI case) and $0.0061 m^2.s^{-2}$ (for the 7% TI case), while the dissipation rate initial condition and inlet is set to $0.000252 m^2.s^{-3}$ for both cases.
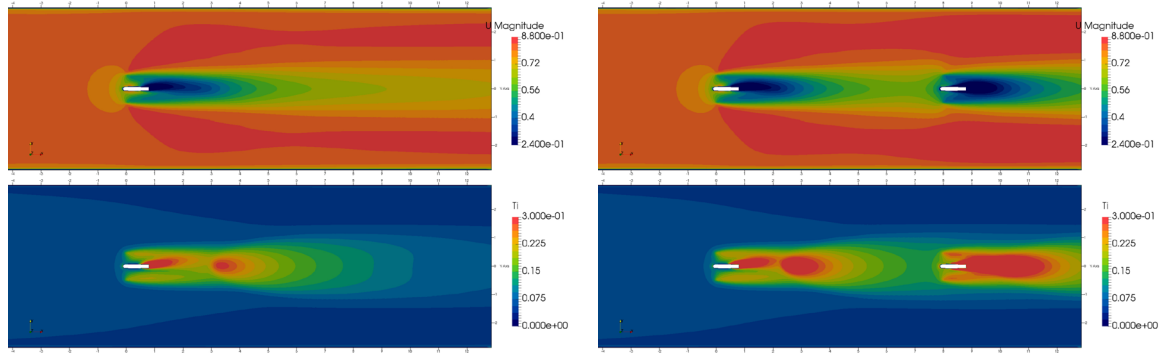
Figure 6: Top images are of velocity magnitude , while the bottom images are of turbulence intensity at 7%. The left images are of the single rotor case, and the right images are of the dual rotor case. All plots are taken in the horizontal plane at hub height, and the axis units are in diameters.

5 RESULTS

5.1 Analytical Wake Field Expression

The algorithms presented in Section 2 are utilised to calculate the mean flow field and turbulence levels behind horizontal axis tidal turbines operating in flows with ambient flow speeds of 0.8 m/s and turbulence intensity values of 3% and 7% (Figures 3 and 4). For these calculations a turbine thrust coefficient of 0.8 is assumed. This fits well with the BEM-CFD results, which show a thrust coefficient of 0.74 at a tip speed ratio (TSR) of 4 at the centre turbine. Since these equations model the far-wake field which typically starts around five diameters downstream only distances beyond this are shown. These figures show that for both turbulence intensities, the wake deficit persists much further downstream than the increased turbulence intensity values in the wake field. Figure 3 shows that the velocity in the far wake is lower and persists longer for lower turbulence intensities. It also shows that the wake field is narrower for lower turbulence intensities. Figure 4 suggests that at 5 diameters downstream the turbulence intensity values are actually greater for lower ambient turbulence intensities. It also suggests that turbulence intensity values nearly reach their ambient values at 13 diameters downstream for both of the evaluated ambient turbulence intensities. The power produced at eight diameter downstream is 39% of upstream power for experimental case [21], whereas the corresponding value for BEM-CFD model that allows TI dissipation is 37% and the analytic wake model is 46%.

5.2 BEM-CFD

The results for all cases converged with a residual less than 0.001. Convergence was achieved between approximately 300 and 1000 iterations depending on the case. All cases are decomposed into eight threads for processing, and total time to convergence ranged between approximately 300 to 900 seconds.

Figure 5 shows velocity magnitude and turbulence intensity plots at 0.8m/s inlet velocity, and 3% turbulence intensity measured at the centre rotor. The two cases shown in Figure 5 are single rotor running with a TSR of 3.67, and the dual rotor case where the centre rotor is set at a TSR of 4, and a rear rotor (8 diameters downstream) is set to a TSR of 3.67. It can
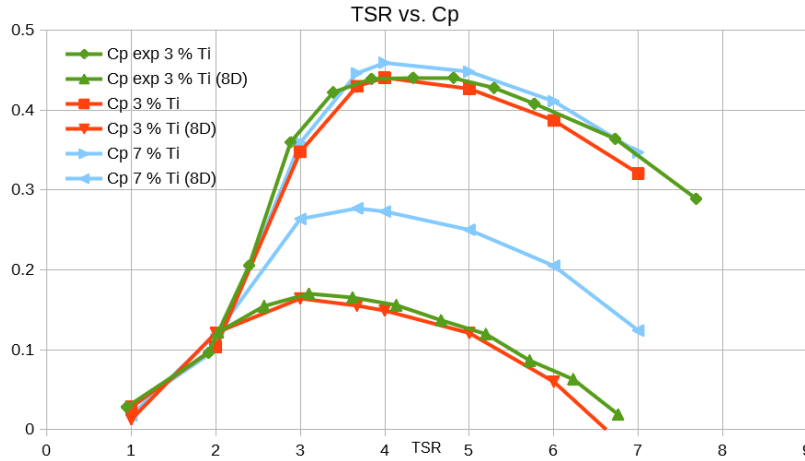
Figure 7: This graphic shows plots of the centre rotor and the '8D' rear rotor (with the centre rotor held to a TSR of 4) for a range of tip speed ratios (TSR). Both experimental results from [21], and BEM-CFD results are shown in this visualisation.

be observed that the velocity deficit behind the centre rotor is greater when the rear rotor is placed downstream. This phenomena is also observed in the TI plots. The single rotor plots compare favourably with the equivalent velocity and turbulence plots from [3], including the asymmetry of the wake caused by the interaction of the tower assembly with the wake rotation. This observation is not made in [1] as the assembly structure is not modelled.

Figure 6 shows the same case as in Figure 5, with the turbulence increased to achieve 7% at the centre rotor. The same trends can be observed for TI set to 7% as described for TI set to 3%. The notable differences include; a shorter wake recovery distance, and a movement upstream of the turbulence pooling in the centre of the wake. This improved wake recovery has a knock on effect on the downstream performance of the rotor.

The rotor performances shown in Figure 7 demonstrate the single rotor performance (Cp) compared to TSR and dual rotor performance (Cp of the downstream rotor) for the two turbulence cases. The upstream rotor is held at a TSR of 4. It is observed there's a significant increase in downstream turbine performance at higher turbulence levels. This corresponds well with the trends observed in [21] when moving from 3% to 15% TI. It is noted that in [3] there is a small drop in performance when comparing the 3% case with the 15% case at the centre rotor, however, this is not observed in our results for the centre turbine when comparing 3% to 7% TI.

6 CONCLUSIONS

The BEM-CFD TSR sweep results (Figure 7) show good correlation with the experiments in [3] and [21]. The velocity and turbulence profiles in Figure 5 show similarly good correlation, which gives us confidence in the higher turbulence ($TI = 7\%$) results shown in Figure 6. The results from the analytical wake field expressions show similar correlation (Figures 3 and 4) with the experimental results, and the BEM-CFD plots in 5 and 6.

From the results it can be seen that as free stream turbulence increases, the distance at which

the wake recovers to free stream velocity significantly reduces. This result is expected, however of note is that both models capture this with a useful level of accuracy. The CFD model provides a more asymmetric distribution of the velocity and turbulence fields, this is due to simulating the tower structure within the CFD domain. Another effect of this is the 'pooling' of higher turbulence at the 6 diameter downstream location (see Figures 5 and 6). This accumulation is the result of the tower drag wake mixing with the rotating turbine wake.

There is no drop in performance (although expected) at the front turbine when turbulence increases. This is likely due to the lift and drag curves not reflecting a change in characteristics as turbulence increases. This could also explain a small error in the rear turbine performance profile (Figure 7).

The BEMT analytical wake expression model provides a symmetric wake profile; the tower structure is not modelled in this type of simulation. The wake recovery and profile are consistent with experiment and BEM-CFD, demonstrating the effectiveness of this approach, and the future potential of computationally efficient turbine array prediction.

7   Acknowledgements

REFERENCES

[1] M. Edmunds, A. J. Williams, I. Masters, and T. N. Croft, "An enhanced disk averaged CFD model for the simulation of horizontal axis tidal turbines," *Renewable Energy*, vol. 101, pp. 67 – 81, 2017. [Online]. Available: http://www.sciencedirect.com/science/article/pii/S096014811630708X

[2] J. H. VanZwieten, P. Pyakurel, T. Ngo, C. Sultan, and N. I. Xiros, "An assessment of using variable blade pitch for moored ocean current turbine flight control," *International Journal of Marine Energy*, vol. 13, pp. 16–26, 2016.

[3] P. Mycek, B. Gaurier, G. Germain, G. Pinon, and E. Rivoalen, "Experimental study of the turbulence intensity effects on marine current turbines behaviour. Part I: One single turbine," *Renewable Energy*, vol. 66, no. 0, pp. 729 – 746, 2014.

[4] P. Pyakurel, W. Tian, J. H. VanZwieten, and M. Dhanak, "Characterization of the mean flow field in the far wake region behind ocean current turbines," *Journal of Ocean Engineering and Marine Energy*, pp. 1–11, 2017.

[5] P. Pyakurel, "Numerical simulation of an ocean current turbine operating in a wake field."

[6] G. C. Larsen, *A simple wake calculation procedure*, 1988.

[7] J. F. Ainslie, "Calculating the flowfield in the wake of wind turbines," *Journal of Wind Engineering and Industrial Aerodynamics*, vol. 27, no. 1-3, pp. 213–224, 1988.

[8] N. O. Jensen, *A note on wind generator interaction*, 1983.

[9] H. G. Weller, G. Tabor, H. Jasak, and C. Fureby, "A tensorial approach to computational continuum mechanics using object-oriented techniques," *Computers in Physics*, vol. 12, no. 6, pp. 620–631, 1998.

[10] B. Launder and D. Spalding, *Mathematical models of turbulence, 1972.* Academic Press, London, 1972.

[11] V. Yakhot, S. Orszag, S. Thangam, T. Gatski, and C. Speziale, "Development of turbulence models for shear flows by a double expansion technique," *Physics of Fluids A: Fluid Dynamics (1989-1993)*, vol. 4, no. 7, pp. 1510–1520, 1992.

[12] I. Abbott and A. Von Doenhoff, *Theory of Wing Sections, Including a Summary of Airfoil Data*, ser. Dover Books on Aeronautical Engineering Series. Dover Publications, 1959, no. 1.

[13] A. Bahaj, A. Molland, J. Chaplin, and W. Batten, "Power and thrust measurements of marine current turbines under various hydrodynamic flow conditions in a cavitation tunnel and a towing tank," *Renewable energy*, vol. 32, no. 3, pp. 407–426, 2007.

[14] F. Maganga, G. Germain, J. King, G. Pinon, and E. Rivoalen, "Experimental characterisation of flow effects on marine current turbine behaviour and on its wake properties," *IET Renewable Power Generation*, vol. 4, no. 6, pp. 498–509, 2010.

[15] T. ODoherty, A. Mason-Jones, D. M. ODoherty, P. S. Evans, C. Wooldridge, and I. Fryett, "Considerations of a horizontal axis tidal turbine," *Proceedings of the ICE-Energy*, vol. 163, no. 3, pp. 119–130, 2010.

[16] J. Chapman, I. Masters, M. Togneri, and J. Orme, "The buhl correction factor applied to high induction conditions for tidal stream turbines," *Renewable Energy*, vol. 60, no. 0, pp. 472 – 480, 2013. [Online]. Available: http://www.sciencedirect.com/science/article/pii/S0960148113002632

[17] I. Masters, R. Malki, A. J. Williams, and T. N. Croft, "The influence of flow acceleration on tidal stream turbine wake dynamics: A numerical study using a coupled bem–cfd model," *Applied Mathematical Modelling*, vol. 37, no. 16, pp. 7905–7918, 2013.

[18] R. Malki, A. Williams, T. Croft, M. Togneri, and I. Masters, "A coupled blade element momentum–computational fluid dynamics model for evaluating tidal stream turbine performance," *Applied Mathematical Modelling*, vol. 37, no. 5, pp. 3006–3020, 2013.

[19] L. Lavaroni, S. J. Watson, M. J. Cook, and M. R. Dubal, "A comparison of actuator disc and BEM models in CFD simulations for the prediction of offshore wake losses," in *Journal of Physics: Conference Series*, vol. 524, no. 1. IOP Publishing, 2014, p. 012148.

[20] Q. Guo, L. Zhou, and Z. Wang, "Comparison of bem-cfd and full rotor geometry simulations for the performance and flow field of a marine current turbine," *Renewable Energy*, vol. 75, pp. 640–648, 2015.

[21] P. Mycek, B. Gaurier, G. Germain, G. Pinon, and E. Rivoalen, "Experimental study of the turbulence intensity effects on marine current turbines behaviour. Part II: Two interacting turbines," *Renewable Energy*, vol. 68, no. 0, pp. 876 – 892, 2014.